Desalination and Water Treatment
www.deswater.com

doi: 10.5004/dwt.2021.26804

216 (2021) 389–400
March

Synthesis of Ni-Co-CNT nanocomposite and evaluation of its photocatalytic dye (Reactive Red 120) degradation ability using response surface methodology

Atefeh Shokrgozar[a,b], Kumars Seifpanahi-Shabani[c], Bahaaddin Mahmoodi[d], Niyaz Mohammad Mahmoodi[b,*], Farhad Khorasheh[a], Morteza Baghalha[a]

[a]*Department of Chemical and Petroleum Engineering, Sharif University of Technology, Tehran, Iran, Tel. +98 21 22969771; Fax: +98 21 22947537; emails: Shokrgozar.atefeh@gmail.com (A. Shokrgozar), khorashe@sharif.ir (F. Khorashe), baghalha@sharif.edu (M. Baghalha)*
[b]*Department of Environmental Research, Institute for Color Science and Technology, Tehran, Iran, email: mahmoodi@icrc.ac.ir*
[c]*Faculty of Mining, Petroleum and Geophysics Engineering, Shahrood University of Technology, Shahrood, Iran, email: seifpanahi@shahroodut.ac.ir*
[d]*Department of Environmental Science and Engineering, Faculty of Natural Resources, University of Tehran, Karaj, Iran, email: mahmoodi.b@ut.ac.ir*

Received 4 January 2020; Accepted 10 November 2020

ABSTRACT

Herein, NiO and Co_2O_3, $NiCo_2O_4$, and $NiCo_2O_4$/multi-walled carbon nanotubes nanocomposite were synthesized by the hydrothermal method and characterized by scanning electron microscopy, energy dispersive spectroscopy, and X-ray diffraction. The photocatalytic activity of the synthesized materials was evaluated by Reactive Red 120 dye degradation. The photocatalytic activity of NiO and Co_3O_4 was enhanced not only by the formation of $NiCo_2O_4$, but also by its interaction with the functionalized multiwall carbon nanotubes support. The response surface methodology (RSM) was used to obtain the optimum parameters, including catalyst dosage, initial dye concentration, and pH on the dye degradation and reduction in total organic compounds (TOC). The dye removal and TOC reduction under optimum conditions (catalyst dose of 0.01 g, pH of 3, and dye concentration of 20 ppm) were 88.9% and 48.7%, respectively.

Keywords: Ni-Co-CNT nanocomposite; Synthesis and characterization; Photocatalytic dye degradation

1. Introduction

The increasing global population with limited water sources has led to the need for the development of new technologies to treat industrial and domestic effluents. It is estimated that over 50% of pollutants entering the water sources are organic contaminants. According to recent reports, over 0.7 million tons of dyestuffs are produced and consumed in different industries, including textile, paper, leather, foods, and cosmetics. The textile industry alone uses some 21–377 m^3 of water for every ton of textile products during the dyeing and finishing processes, with more than 280,000 tons of textile dyes being discharged into water [1–12]. Since synthetic dyes are a severe hazard to the environment, human health, and marine life, in the last decade, researches have been focused on the development of technologies capable of the treatment of these organic pollutants [13].

Traditionally, the dye treatment methods are categorized in physical, biological, and chemical processes [14–18].

* Corresponding author.

Physical methods merely transfer the contaminants from one medium to another, requiring an additional treatment method for purification of the second media [19]. Most of the physical treatment processes are also challenging to control and are costly in large-scale applications [20]. Furthermore, dye production industries place a great emphasis on the production of complex dyestuffs with lasting properties that result in dyes that are poorly biodegradable [21].

Semiconductor photocatalysis has been used as an advanced oxidation process for the degradation of dye pollutants. The excited electrons and positive holes can initiate reduction and oxidation reactions, respectively. Eventually, oxidizing agents such as hydroxyl radicals are formed to attack the dye molecules to degrade them quickly and non-selectively [22–24]. The photocatalytic degradation process has many substantial advantages, the most significant one being its capability for complete mineralization of the dye pollutant to species such as water, oxygen, carbon dioxide, and mineral acids [1,2,13].

A composite material prepared from two different metal oxides often shows improved photocatalytic activity for different applications [25]. Nickel oxide is a transition metal with a broad bandgap of 3.6–4.0 eV, which makes it suitable for various applications [26–29]. Numerous studies have focused on the synthesis of NiO composites, including NiO-TiO_2 [30], NiO-ZnO [31], NiO-SnO_2 [32], and NiO-Bi_2O_3 [33] for photocatalytic degradation of organic dye pollutants. Co_3O_4, which is a *p*-type transition metal, has only received limited attention in photocatalytic applications [34–37] and only a few studies have reported the photocatalytic performance of Co_3O_4 composites in dye degradation including Co_3O_4-ZnO [38], Co_3O_4-Cu_2O [39], and Co_3O_4-Ag_2S [40].

Carbon materials are known as appropriate electron acceptor supports that can strongly suppress the electron–hole recombination [41]. Among the carbon materials, multi-walled carbon nanotubes (MWCNTs) have desirable physical, electrical, chemical, and thermal characteristics [42,43]. Many attempts have recently been made to synthesize carbon nanotube (CNT)-supported composites, including TiO_2/MWCNTs [44–47], ZnO/CNTs [48], and CeO_2/CNTs [49] that have pointed to enhanced photocatalytic activity in the presence of CNTs.

A literature review indicated that photocatalytic dye degradation was not investigated by Ni-Co-CNT nanocomposite in detail. Herein, $NiCo_2O_4$ nanocomposite on functionalized MWCNT was synthesized as a novel photocatalyst. Reactive Red 120 (RR120) was chosen as a dye model. Reactive dyes are the most important in the textile industry for dyeing cotton. Their annual production is estimated to more than 120,000 tons [50]. RR120 is a typical reactive azo anionic dye, potentially carcinogenic, mutagenic, and allergenic on exposed organisms because of its metabolites (e.g., aromatic amines). RR120 is more stable and has lower biodegradability in aqueous solutions than other types of dyes [51]. The photocatalytic activity of $NiCo_2O_4$/MWCNT under UV irradiation for degradation of Reactive Red 120 was compared with those $NiCo_2O_4$, NiO, and pure Co_3O_4.

2. Materials and methods

2.1. Materials

Reactive Red 120 was obtained from Ciba and used without further purification. The molecular structure of RR120 is shown in Fig. 1. Urea which was used as the oxidizing agent, the precursor salts $Co(NO_3)_2{\cdot}6H_2O$ and $Ni(NO_3)_2{\cdot}6H_2O$, and ethanol were obtained from Merck (Germany). H_2SO_4 (95%–98%) and HNO_3 (65%) were also obtained from Merck and used to functionalize the MWCNT surface. The initial pH of dye solutions was adjusted to the desired values by H_2SO_4 (95%–98%), and NaOH (≥99%) purchased from Merck.

2.2. Characterization tests

Fourier transform infrared spectroscopy (FTIR) using a Perkin-Elmer spectrophotometer (lambda 25 – the USA) was used to determine the functional groups present on the surface of MWCNTs. The crystalline phases of the synthesized nanoparticles were analyzed by examining their X-ray diffraction (XRD) patterns recorded by X'Pert PRO MPD instrument from PANalytical Company (Netherlands) with Cu Kα radiation (λ = 1.5406 A). Scanning electron microscopy (SEM) was performed using a LEO 1455VP (USA) to determine the morphology of the synthesized nanostructures. Energy dispersive spectroscopic (EDS) analysis was performed by a Tescan Vega instrument (Czech Republic) to evaluate the chemical composition of $NiCo_2O_4$/MWCNT nanocomposite to demonstrate that the expected elements were anchored on the surface of MWCNT. Moreover, the bandgap energy of nanoparticles was determined using diffuse reflectance spectroscopy (DRS) analysis using an Avaspec 2048 TEC instrument (Netherlands) equipped with an AvaLamp DH-S setup.

2.3. Catalyst preparations

The NiO nanoparticles were prepared by simple hydrothermal precipitation method followed by calcination. One millimole of $Ni(NO_3)_2{\cdot}6H_2O$ and 0.3 g of urea was

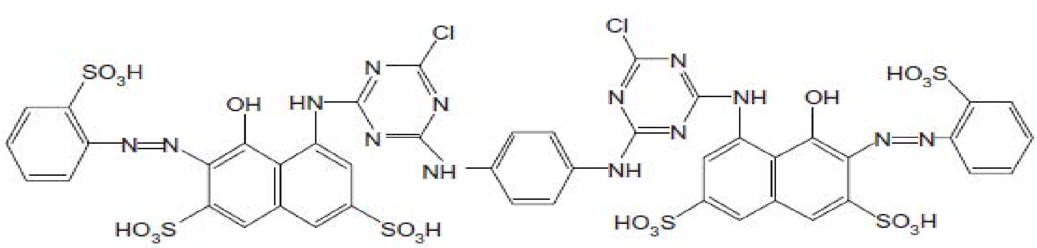

Fig. 1. Molecular structure of RR120 dye.

dispersed in 40 mL of a solution containing a volume ratio of deionized water to ethanol of 1–4. The mixture was then placed into an autoclave and was heated at 80°C for 14 h. The mixture was subsequently centrifuged and washed several times. The precipitant was then dried in an oven at 60°C. The resulting solid was then calcined at 400°C using a temperature ramp of 2°C/min and maintained at that temperature for 3 h. The Co_3O_4 nanoparticles were synthesized using a similar procedure as that used for the synthesis of NiO. For the synthesis of $NiCo_2O_4$ nanoparticles, 1 mmol of precursor salts with 2:1 molar ratio of $Co(NO_3)_2$ to $Ni(NO_3)_2$ and 0.3 g of urea was dispersed in 40 mL of a solution containing a volume ratio of deionized water to ethanol of 1–4. The subsequent preparation steps were similar to those described for NiO synthesis. Pristine CNT surface is quite inert, requiring it to undergo treatments to create defects and active sites for metal particles to be anchored on its surface. Oxidation by strong acids is an effective strategy to create carboxylic (–COOH) and hydroxylic (–OH) functional groups on the external surface of CNTs [52]. For the synthesis of $NiCO_2O_4$/MWCNT composite, the MWCNTs were first functionalized using the methodology described in the literature [52]. This methodology is as follows: 1 g of pristine MWCNTs and 100 mL of the acid mixture (75 mL of H_2SO_4 97% with 25 mL HNO_3 65%) were mixed, and the suspension was heated in a flask under constant agitation at 50°C for 8 h. The mixture was then allowed to cool to room temperature. The mixture was subsequently filtered and washed several times until obtaining a neutral pH. Finally, the filtered residue was dried at 100°C. The functionalized MWCNT hereafter is named f-MWCNT.

The f-MWCNTs (6 mg) was dispersed and sonicated in 5 mL of ethanol, and the resulting suspension was added to the precursor solution. The black suspension was further sonicated and transferred into an autoclave and heated at 80°C for 14 h. After washing and centrifuging, the black precipitate was dried at 60°C and subsequently calcined at 400°C with a temperature ramp of 2°C/min and maintained at that temperature for 3 h.

2.4. Dye degradation

The degradation of RR120 in an aqueous solution under UV radiation was performed in a batch photoreactor. The source of UV radiation (UV-C) was a Philips (Netherlands) UV-lamp (9 W) placed in the center of the reaction vessel. The external surface of the reactor was completely covered by aluminum foils to maximize irradiation in the reaction media. At the beginning of each experiment, 500 mL of a solution with a specified dye concentration was mixed with a specified amount of photocatalyst. The effect of pH on the photodegradation of RR120 was investigated in the pH range 3–11. The solution pH was adjusted by adding 0.1 M H_2SO_4 or 0.1 M NaOH solutions to reach the desired pH value prior to irradiation. During the reaction, the solution containing the photocatalyst particles was well agitated inside the reactor. The suspension was first stirred for 30 min in darkness to ensure the adsorption–desorption equilibrium of the dye molecules on the catalyst surface. At different time intervals, a 10 mL sample was taken from the solution media. The photocatalyst particles were separated from the sample by centrifuging. The dye concentration was measured using a UV-vis spectrophotometer (Perkin-Elmer) from the optical absorption peak of RR120 at 536 nm. The percent dye removal was calculated as follows:

$$\text{Dye removal}\left(\%\right)=\left[\frac{\left(A_0-A_t\right)}{A_0}\right]\times 100 \tag{1}$$

where A_0 and A_t are the initial and the measured dye absorptions, respectively. The total organic carbon (TOC) of the solution was measured by a Shimadzu TOC analyzer (Japan). To determine the optimum operating conditions, TOC, and dye removal were determined by varying the following three factors with their corresponding ranges; catalyst dosage (0.02–0.06 g/L), initial dye concentration (20–40 ppm), and pH (3–11), using central composite design (CCD) by Design Expert software.

3. Results and discussion

3.1. Catalyst characterizations

In order to confirm the presence of different functional groups on the MWCNT surface resulting from acid treatment, FTIR spectra of both pristine MWCNT and functionalized MWCNT were obtained and are presented in Fig. 2. The functionalized MWCNT spectrum showed some wide and sharp characteristic peaks were attributed to oxygen-containing groups, while these peaks were relatively weak in the spectrum for pristine MWCNT. The peaks located at 3,436 and 1,651 cm^{-1} were assigned to hydroxyl and carbonyl groups, respectively, and they were more dominant for functionalized MWCNT. As expected, acid treatment had led to –COOH groups on the CNT surfaces [53,54]. The peaks around 3,400 cm^{-1} can also appear due to the adsorption of atmospheric moisture on the CNT surface [52,55]. The characteristic peak appearing at 1,634 cm^{-1} illustrates the absorbance of double band C=C in the pristine CNT spectrum.

The functionalized MWCNT spectrum did not possess the C=C characteristic peak but contained a new peak at 1,651 cm^{-1} that was due to the oxidation of double band carbon during acid treatment that led to the formation of carboxyl group [56,57]. The peak appearing at 1,384 cm^{-1} is associated with C–C vibration band [58]. In both pristine and oxidized CNT spectra, the peak around 2,921 cm^{-1} indicated the presence of –CH bond on the CNT surfaces, indicating some structural defects having remained on the CNT surface during the manufacturing process [57].

Fig. 3 demonstrates the surface morphology, shape, and size of NiO, Co_3O_4, $NiCo_2O_4$, and $NiCo_2O_4$/MWCNT nanocomposite obtained by SEM analysis. The micrograph presented in Fig. 3b appears to indicate the flower-like formation of Co_3O_4 nanoparticles. Comparison of Figs. 3a–c indicates that the shape of NiO and Co_3O_4 particles do not appear to have changed for $NiCo_2O_4$ nanocomposite. The micrograph of $NiCo_2O_4$/MWCNT presented in Fig. 3d confirms the direct surface connection between CNT and $NiCo_2O_4$.

EDS analysis was performed to confirm the presence of different elements and approximate their composition in

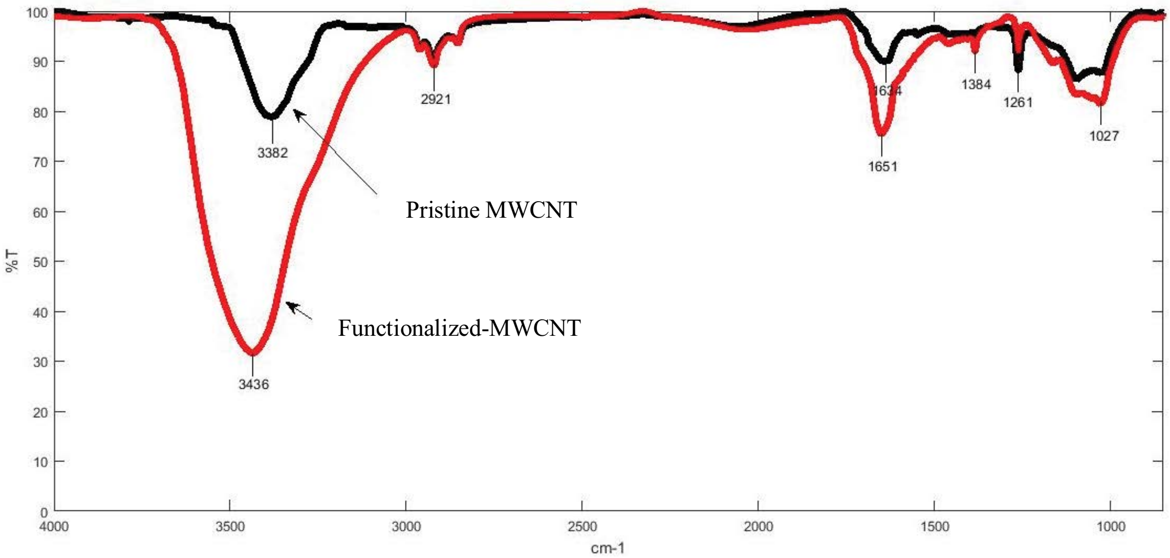

Fig. 2. FTIR spectrum of pristine MWCNT and f-MWCNT.

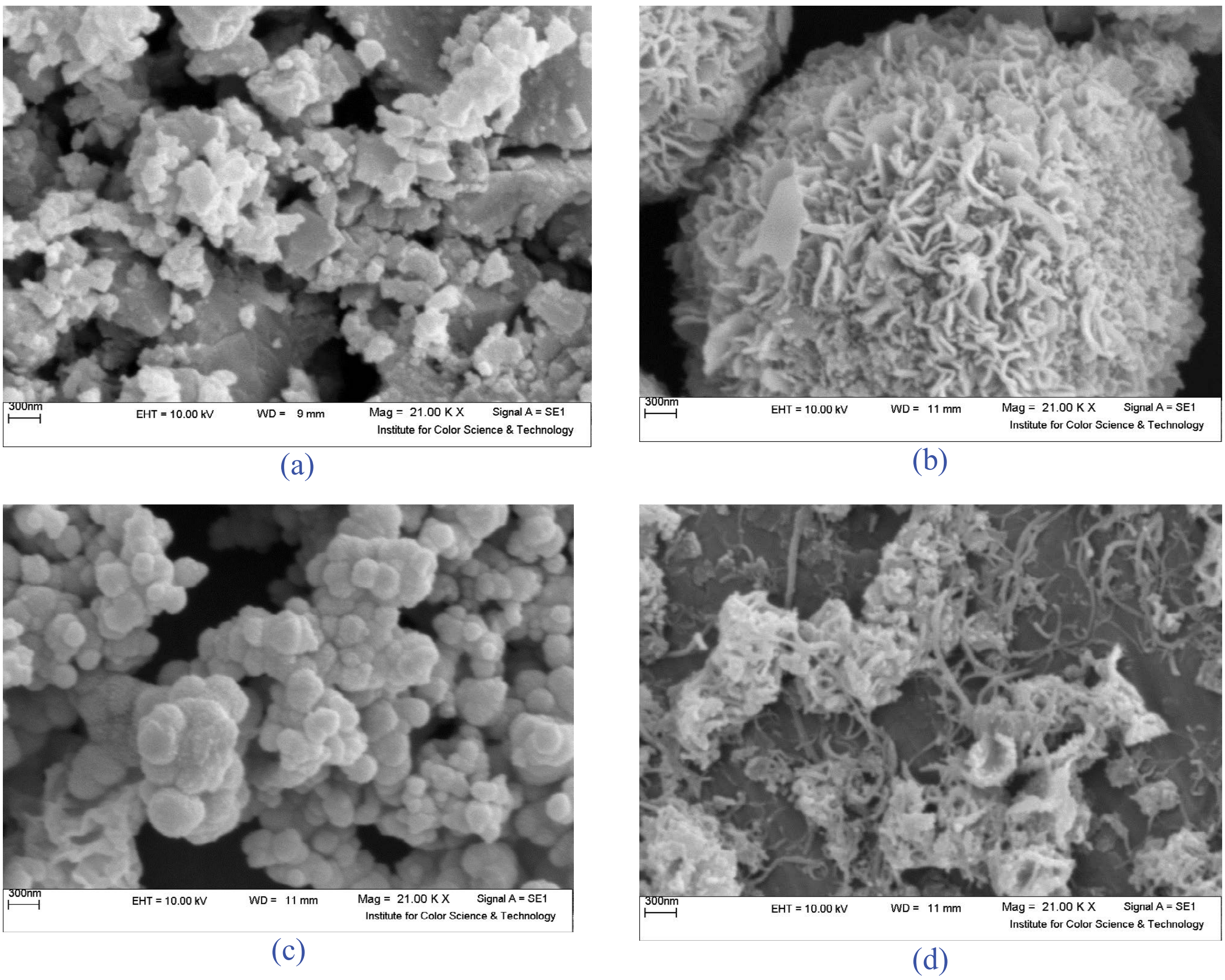

Fig. 3. SEM images (a) NiO, (b) Co_3O_4, (c) $NiCo_2O_4$, and (d) $NiCo_2O_4$/MWCNT.

$NiCo_2O_4$/MWCNT nanocomposite. EDS results indicated the presence of elements C, O, Co, and Ni. The quantitative analyses in terms of weight percentages for each element are reported in Fig. 4, confirming a good agreement with expected values.

Crystalline structure, phase purity, and average crystalline size were obtained by XRD analysis. The XRD patterns for NiO, Co_3O_4, $NiCo_2O_4$, and $NiCo_2O_4$/MWCNT nanoparticles are presented in Fig. 5. The XRD pattern of synthesized NiO exhibited five characteristic diffraction peaks, which were located at 2θ of 37.3°, 43.4°, 63°, 75.6°, and 79.6° that are related to (111), (200), (220), (311), and (222) planes, respectively. The NiO pattern is matched with ICCD card 01-075-0197 that belongs to NiO in cubic crystalline structure with a lattice parameter of 4.17 Å.

The XRD pattern of synthesized Co_3O_4 exhibited peaks located at 2θ of 19°, 31°, 36°, 38°, 44°, 55°, 59°, 65°, and 78°, corresponding to planes (111), (220), (311), (222), (400), (422), (511), (440), and (622), respectively, which is matched with ICCD card 01-076-1802 for Co_3O_4 in cubic crystalline structure with a lattice parameter of 8.072 Å. The $NiCo_2O_4$ pattern is matched with ICCD card 01-073-1702, belonging to $NiCo_2O_4$ in cubic form and lattice parameter of 8.114 Å. The characteristic peaks which were observed in $NiCo_2O_4$ XRD pattern at 2θ of 19°, 31.1°, 36.7°, 44.43°, 49.14°, and 64.94° correspond to planes (111), (220), (311), (400), (331), and (440), respectively.

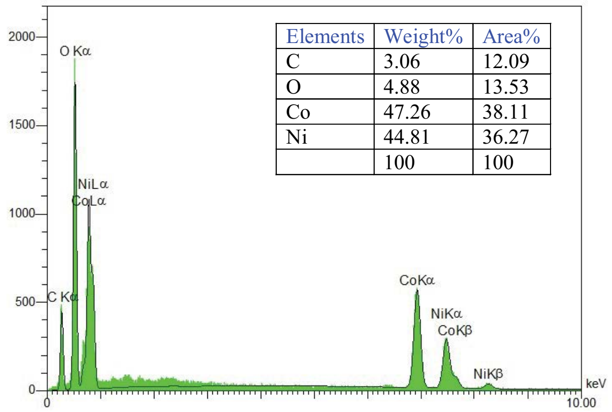

Fig. 4. Elemental composition of $NiCo_2O_4$/MWCNT nanocomposite from EDS analysis.

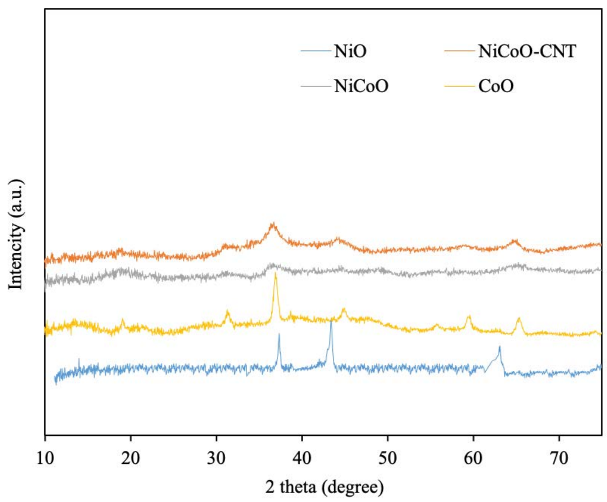

Fig. 5. XRD patterns of NiO, Co_3O_4, $NiCo_2O_4$, and $NiCo_2O_4$/MWCNT.

The XRD pattern for $NiCo_2O_4$/MWCNT nanocomposite exhibited characteristic diffraction peaks at 2θ of 18.78°, 31.07°, 36.56°, 44.33°, 59.07°, and 64.68°. Because of the low quantity of MWCNT in the composite (less than 3 wt.%), as confirmed by EDS analysis, MWCNT peaks were not detected by XRD analysis. However, the $NiCo_2O_4$/MWCNT pattern was in a better agreement with $NiCo_2O_4$ pattern card 01-073-1702 as compared with the XRD pattern of synthesized $NiCo_2O_4$. Moreover, the XRD pattern of $NiCo_2O_4$/MWCNT shows a noticeably higher crystallinity compared with that for synthesized $NiCo_2O_4$. The plates and lattice parameter for both samples, however, were the same. It could, therefore, be concluded that carbon nanotubes materials had provided suitable locations for crystalline structure formation and growth.

The average crystalline size, d, of NiO, Co_3O_4, $NiCo_2O_4$, and $NiCo_2O_4$/MWCNT was estimated by Scherrer's equation as follows:

$$d = \frac{K\lambda}{B\cos\theta} \tag{2}$$

where B is the full width of the observed diffraction peak at its half maximum intensity (FWHM), K is the shape factor (typically taking the value of 0.9), θ is the Bragg angle, and λ is the wavelength of the X-ray source (0.154 nm for Cu $K\alpha$ radiation) [59–62]. The average crystalline sizes calculated by Scherrer's equation are reported in Table 1. $NiCo_2O_4$/MWCNT nanocomposite had the smallest crystalline size. The sharper peaks in $NiCo_2O_4$/MWCNT XRD pattern as compared with $NiCo_2O_4$ confirmed a more proper crystalline formation of $NiCo_2O_4$ on MWCNT support. In a highly crystalline structure, the number of defects (which can be the recombination sites) are lower in $NiCo_2O_4$/MWCNT, making it a more efficient photocatalyst as compared with NiO, Co_3O_4, and $NiCo_2O_4$ [3].

The bandgap is a significant parameter in determining the optical properties of semiconductor materials that is generally determined from the UV-Vis DRS [28]. Tauc plot is widely used to estimate the bandgap (E_g) from the optical absorption spectrum using the following equations [28,63]:

$$\alpha h\nu = A\left(h\nu - E_g\right)^{\gamma} \tag{3}$$

$$h\nu = \frac{hc}{\lambda} = \frac{1,240}{\lambda} \tag{4}$$

where A is a material constant and γ is 1/2 for direct or 2 for indirect transitions. The $h\nu$ is the photoenergy that is calculated by Eq. (4). The α is substituted by Kubelka–Munk function expressed in Eq. (5):

Table 3
Significance of each parameter in dye removal and TOC reduction models

	A	*B*	*C*	*AB*	*AC*	*BC*	*B2*	*C2*
Dye removal%	0.0230	<0.0001	<0.0001	0.0320	–	0.0368	0.0517	<0.0001
TOC reduction%	0.0324	<0.0001	0.0020	0.0507	0.0852	0.0004	0.0001	0.0001

A: Catalyst dosage, *B*: initial dye concentration, and *C:* pH

$$F(R)=\frac{K}{S}=\frac{(1-R)^2}{2R} \quad (5)$$

where R is the reflectance of an infinitely thick specimen. K and S are the absorption and scattering coefficients, respectively [27,64]. By extrapolating the linear region of the $(F(R)\cdot h\nu)^{1/\gamma}$ vs. $h\nu$ plot to $F(R) = 0$, the bandgap (E_g) is obtained [65]. The bandgap of all NiO, Co_3O_4, $NiCo_2O_4$, and $NiCo_2O_4$/MWCNT nanoparticles was evaluated from the above extrapolation as presented in Fig. 6. The optical band gap for NiO was found to be 3.45 eV, which is in good agreement with the 3.5–4 eV range reported in the literature [6,9,13]. The bandgap energy for Co_3O_4 nanoparticles was determined to be 2.1 eV, which is within the range of 1.48–2.19 eV previously reported [34,40]. The Tauc plot for $NiCo_2O_4$ nanocomposite indicated the band gaps of 1.7 and 3.2 eV associated with Co_3O_4 and NiO, respectively, indicating a shift of 0.25 and 0.4 eV to lower bandgap energies for NiO and Co_3O_4, respectively, in comparison with pure NiO and Co_3O_4 nanoparticles. The shift to lower bandgap energies was probably due to the interactions between the semiconductors and the formation of $NiCo_2O_4$ structure [66]. It seems that the formation of $NiCo_2O_4$ nanocomposites has changed the position of valance and conduction bands to reduce the band gaps and improve the optical properties. The bandgap energies of $NiCo_2O_4$/MWCNT nanocomposite were found to be about 1.7 and 3.1 eV for Co_3O_4 and NiO, respectively, indicating a slight improvement in the band gap for NiO that could be due to surface interactions between $NiCo_2O_4$ and MWCNT as evident from SEM micrographs (Fig. 3).

3.2. Photocatalytic performance

Six experiments were performed using 500 mL an initial solution containing 30 ppm of RR120 with a pH of 4.86 to evaluate and compare the photocatalytic activity of 0.01 g NiO, Co_3O_4, $NiCo_2O_4$, or $NiCo_2O_4$/MWCNT. The percentage of dye removals were measured up to 180 min from the start of each experiment, and the results were presented in Fig. 7. The dye removal under UV irradiation without any catalysts reached a maximum of 5.8% after 180 min irradiation indicating that RR120 was highly stable in the absence of any photocatalyst. In four other experiments, 0.0l g of different photocatalysts, including NiO, Co_3O_4, $NiCo_2O_4$, and $NiCo_2O_4$/MWCNT were added to the initial solution, and experiments were performed under UV irradiation. The dye removal after 180 min was 32.16%, 11.15%, 49%, and 67% for NiO, Co_3O_4, $NiCo_2O_4$, and $NiCo_2O_4$/MWCNT, respectively. According to these results, the photocatalytic activity of $NiCo_2O_4$ was higher compared with those for pure NiO and Co_3O_4. Furthermore, the photocatalytic performance of $NiCo_2O_4$/MWCNT was considerably better

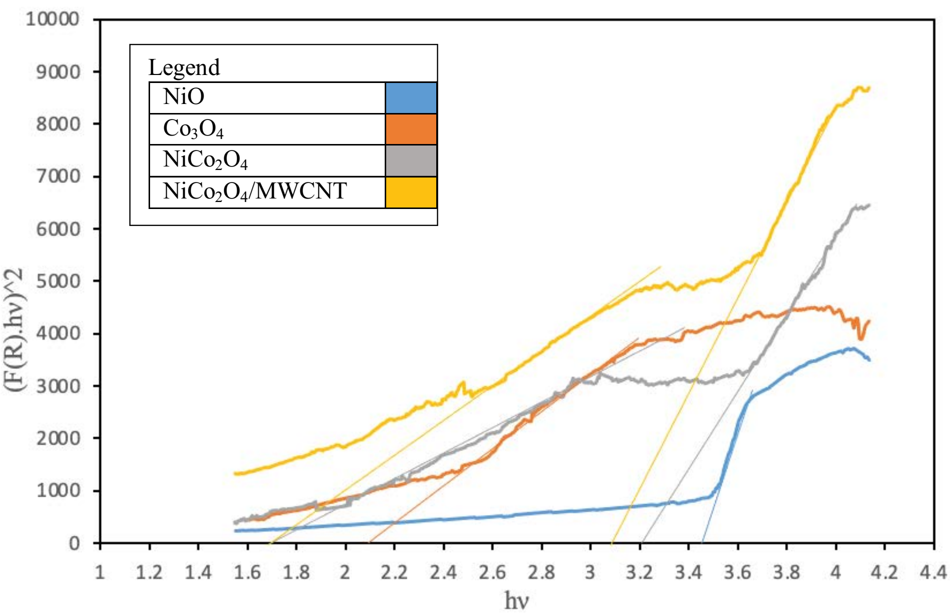

Fig. 6. Tauc plots for NiO, Co_3O_4, $NiCo_2O_4$, and $NiCo_2O_4$/MWCNT.

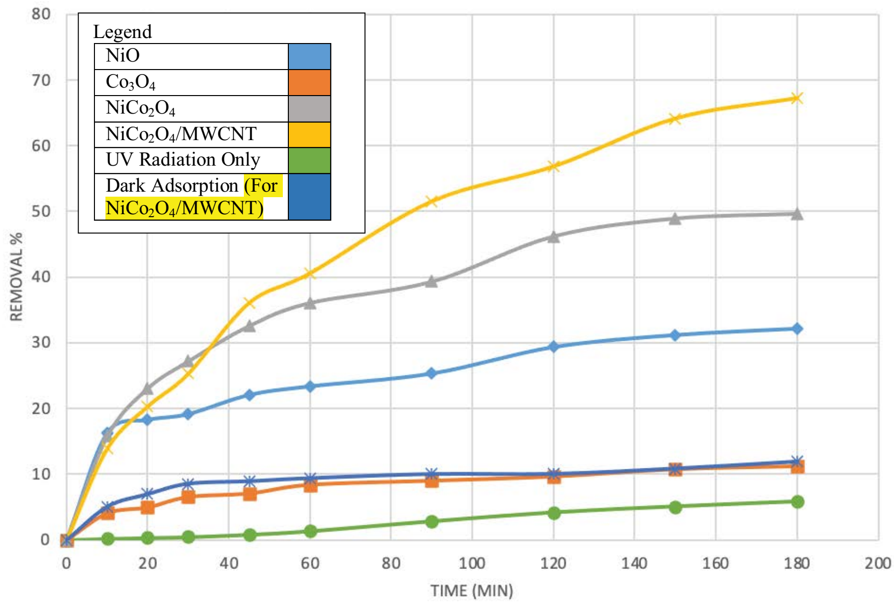

Fig. 7. Comparing the photocatalytic performance of 0.0l g different photocatalysts NiO, Co_3O_4, $NiCo_2O_4$, or $NiCo_2O_4$/MWCNT in 500 mL of RR120 solution with an initial concentration of 30 ppm and natural pH of 4.86 and the adsorption ability of 0.01 g $NiCo_2O_4$/MWCNT in 500 mL of the same solution were evaluated under dark condition. (Note: each experiment has been repeated three times).

than $NiCo_2O_4$. This improvement could be due to the interactions of $NiCo_2O_4$ with MWCNT support, as was evident from DRS analysis that the bandgap energies of $NiCo_2O_4$/MWCNT nanocomposite decreased slightly in comparison with pure NiO and Co_3O_4 nanoparticles and $NiCo_2O_4$ composite. One further experiment was performed using 0.01 g of $NiCo_2O_4$/MWCNT without any UV irradiation to illustrate that the observed dye removal was the result of photocatalytic activity and not simple adsorption.

Twenty experiments were performed using CCD with the above three factors and percentage TOC reduction and dye removal as target functions to investigate the effect of important operating parameters including catalyst dosage, initial dye concentration, and pH on dye removal and TOC reduction by $NiCo_2O_4$/MWCNT. The levels used for the above factors for each experiment, and the responses for each target function are given in Table 2.

The target functions were modeled with second-order polynomials by RSM as follows:

$$\begin{aligned}\text{Dye removal percentage} &= +140.42626 - 657.87500 \\ &\times \text{catalyst dosage} + 0.26112 \times \text{dye concentration} \\ &- 16.81155 \times \text{pH} + 32.26250 \times \text{catalyst dosage} \\ &\times \text{dye concentration} + 0.078094 \times \text{dye concentration} \\ &\times \text{pH} - 0.05419 \times \text{dye concentration}^2 + 0.91520 \times \text{pH}^2\end{aligned} \tag{6}$$

$$\begin{aligned}\text{TOC reduction percentage} &= +52.37992 - 956.75000 \\ &\times \text{catalyst dosage} + 3.94550 \times \text{dye concentration} \\ &- 17.07391 \times \text{pH} + 27.25000 \times \text{catalyst dosage} \\ &\times \text{dye concentration} + 58.75000 \times \text{catalyst dosage} \\ &\times \text{pH} + 0.15375 \times \text{dye concentration} \times \text{pH} - 0.11181 \\ &\times \text{dye concentration}^2 + 0.72617 \times \text{pH}^2\end{aligned} \tag{7}$$

The good accuracy of both models is illustrated in Figs. 8 and 9 in terms of parity plots comparing the actual percentage of dye removal and TOC reduction, respectively, against the predicted values during the photocatalytic degradation of RR120 by $NiCo_2O_4$/MWCNT. Table 3 indicates the significance of each term in the models. Based on $p < 0.0001$, the most significant terms for dye removal are initial dye concentration and the first and second-order effects of pH, while the most important parameter on TOC reduction is the initial dye concentration.

Fig. 10 shows the three-dimensional and contour plots illustrating the effect of independent factors on dependent variables and the interactions of different factors. Fig. 10 demonstrates that the efficiency of dye removal decreases by increasing initial dye concentration. This is commonly observed for photocatalytic dye removal since, under a fixed amount of photocatalyst and the same intensity of UV irradiation, the concentration of degradation agents, namely $OH^\bullet$, $O_2^{-\bullet}$, and h^+, remains constant and insufficient for a high pollutant concentration [67]. Furthermore, for a high dye concentration, the path for a photon to reach the photocatalyst surface is noticeably increased, resulting in lower availability of photons for photocatalytic reactions, thus resulting in a decrease in TOC and dye removal [68]. Since more intermediate products are also generated during the photocatalytic process in a high dye concentration, a competition may exist between the intermediates and dye molecules to access the limited active sites on the photocatalyst surface [69]. Fig. 10 indicates that both TOC reduction and dye removal are weak functions of catalyst dosage and only slightly increase with increasing catalyst dosage.

pH has a strong influence on photocatalytic activity. Fig. 10 indicates how TOC reduction and dye removal change with pH in the range of 3 to 11. For pH < 7, the photocatalytic

Table 1
Average crystalline sizes according to Scherrer's equation

Sample	Maximum intensity peak (2θ degrees)	FWHM (2θ degrees)	Average crystalline size (nm)
NiO	43.38	0.21	80.49
Co_3O_4	36.94	0.41	40.45
$NiCo_2O_4$	36.6	0.35	47.9
$NiCo_2O_4$/MWCNT	36.5	0.5	32.3

activity increases with decreasing pH. This observation can be explained in terms of the point of zero charges (PZC). The photocatalyst surface would become positively charged under acidic conditions allowing for the anionic molecules of RR120 to be adsorbed on the catalyst surface, thus enhancing the photocatalytic degradation improves.

In the alkali region, on the other hand, both dye removal and TOC reduction increased as pH was increased to 11. The probable reason for this observation can be explained in terms of reaction 8 in which holes react with hydroxide anions and produce hydroxide radicals that are strong oxidizing agents [70–73].

$$h_{vb}^{+} + OH^{-} \rightarrow OH^{\bullet} \quad (8)$$

The optimum conditions obtained from CCD were pH of 3, initial dye concentration of 20 mg/L, and 0.01 g dosage of $NiCo_2O_4$/MWCNT nanocomposite. The corresponding percentages for dye degradation and TOC reduction under the optimum conditions were 89.8% and 48.7%, respectively.

4. Conclusions

In this work, NiO, Co_3O_4, $NiCo_2O_4$, and $NiCo_2O_4$/MWCNT were synthesized, characterized, and used as photocatalysts for RR120 dye degradation and mineralization. The experimental tests showed that the photocatalytic activity of $NiCo_2O_4$/MWCNT was higher than NiO, Co_3O_4, and $NiCo_2O_4$. The effects of catalyst dosage, initial dye concentration, and pH on photocatalytic dye degradation using $NiCo_2O_4$/MWCNT were investigated by a CCD analysis. The optimum conditions were found to be initial dye concentration of 20 mg/L, pH of 3, and catalyst dosage of 0.01 g that resulted in 89.8% dye removal and 48.7% TOC reduction after 180 min of UV irradiation.

Table 2
Experimental design and the responses based on experiments proposed by CCD for photocatalytic degradation of RR120 by $NiCo_2O_4$/MWCNT

Run	Factor 1 *A*: catalyst dosage (g)	Factor 2 *B*: initial dye concentration (ppm)	Factor 3 *C*: pH	Response 1 dye removal %	Response 2 TOC reduction %
1	0.03	20	3	91.0	43.7
2	0.02	20	7	62.0	21.0
3	0.02	30	7	53.7	21.2
4	0.02	30	7	60.6	25.0
5	0.01	40	3	51.0	8.0
6	0.03	40	11	54.0	20.0
7	0.02	30	7	58.2	22.0
8	0.01	40	11	45.1	7.0
9	0.03	30	7	58.2	28.0
10	0.02	30	3	71.0	39.6
11	0.01	30	7	53.0	15.0
12	0.03	40	3	67.9	13.0
13	0.02	30	11	69.4	32.0
14	0.02	30	7	60.0	30.0
15	0.02	30	7	60.0	26.5
16	0.02	30	7	56.7	23.0
17	0.01	20	3	93.0	51.0
18	0.01	20	11	68.6	24.0
19	0.02	40	7	40.0	5.0
20	0.03	20	11	70.6	27.5

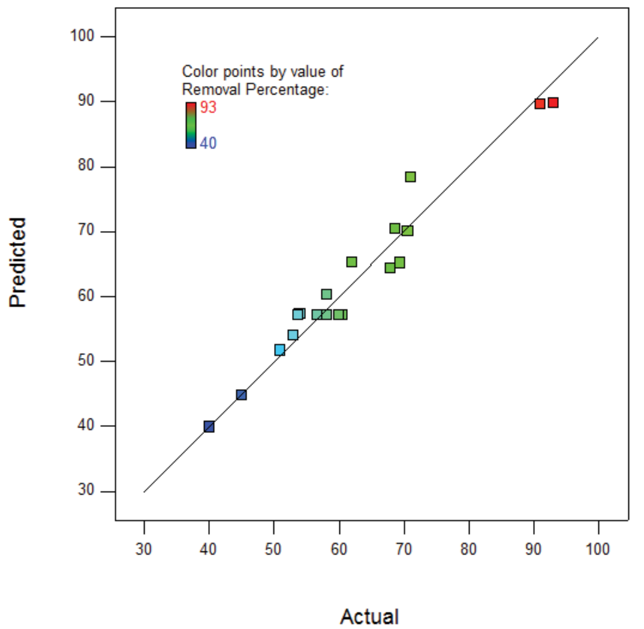

Fig. 8. Predicted against actual values of dye removal for degradation of RR120.

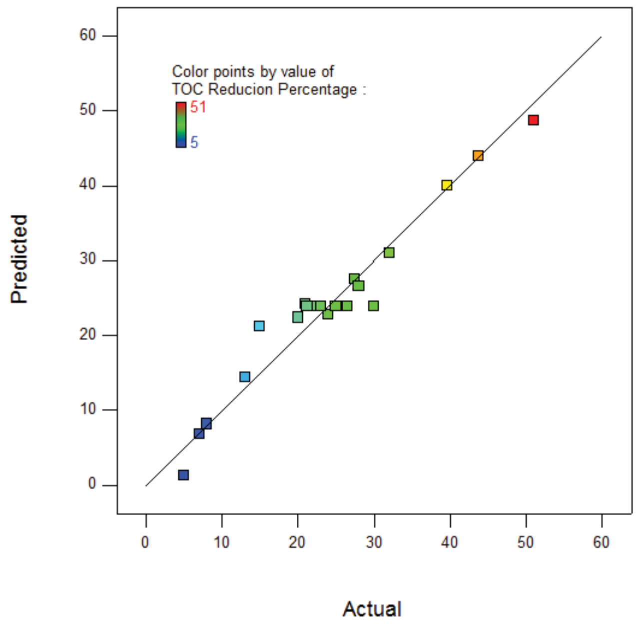

Fig. 9. Predicted against actual values of TOC reduction for degradation of RR120.

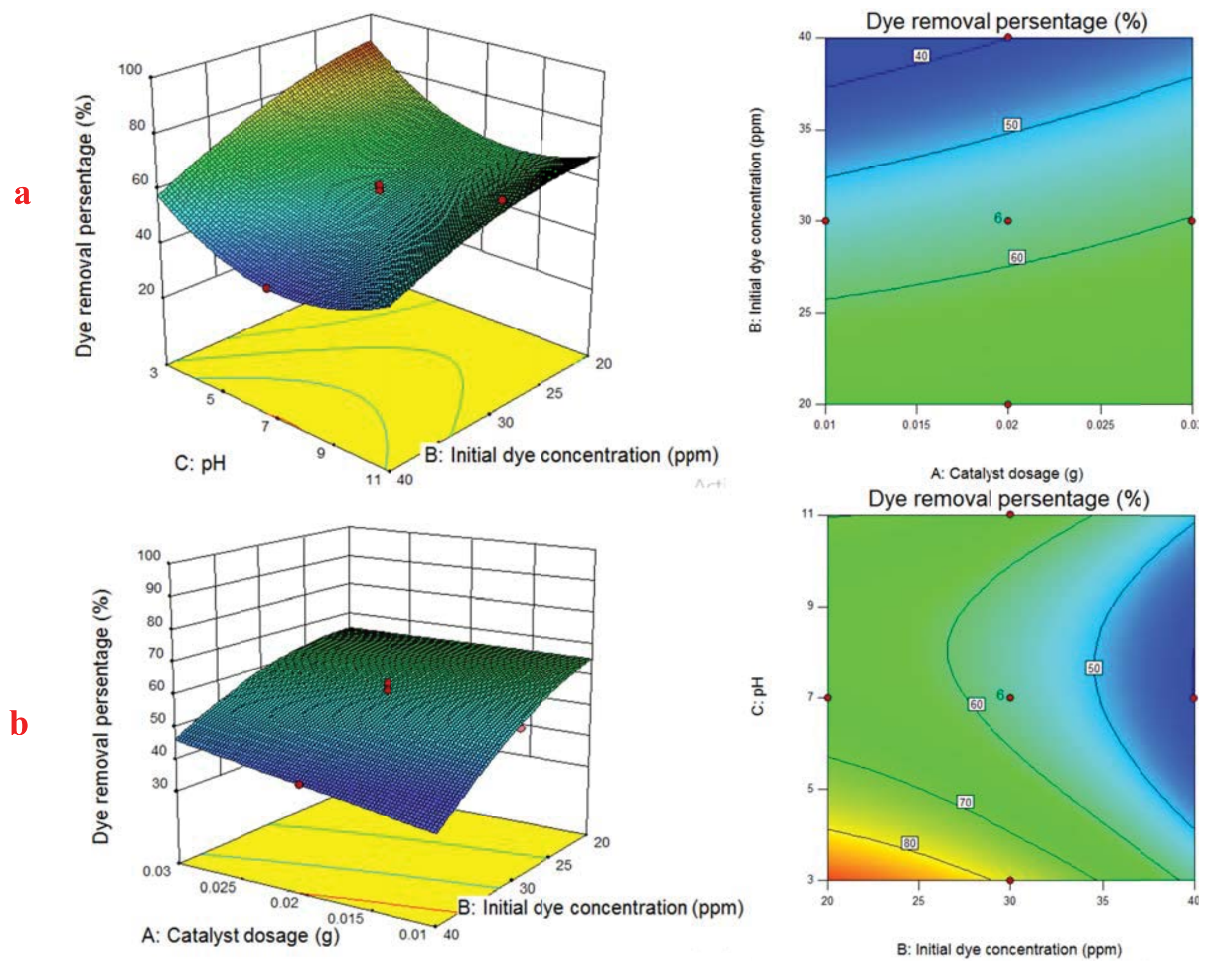

Fig. 10. *Continued*

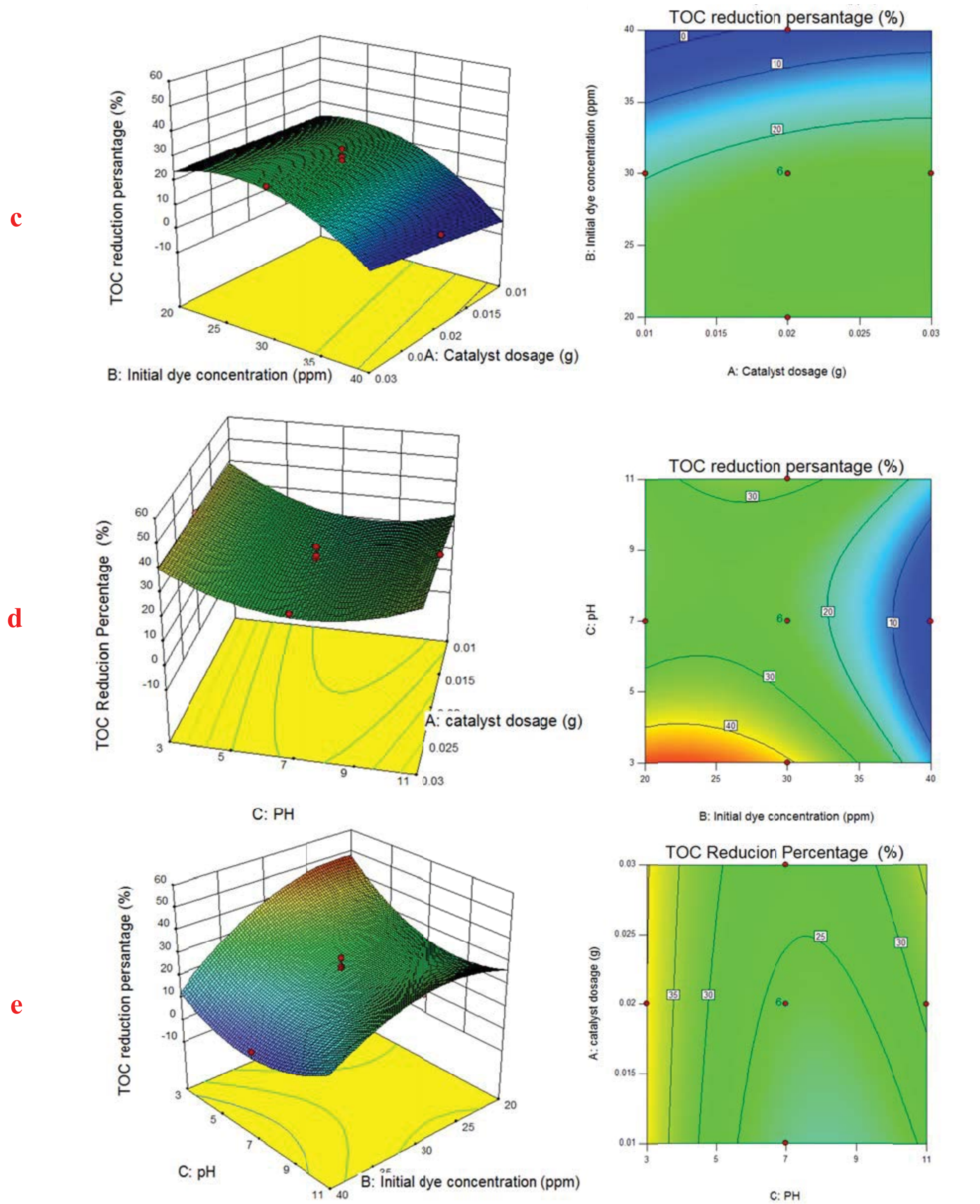

Fig. 10. Three-dimensional (3D) and contour (2D) plots of the predicted responses for dye removal and TOC reduction in degradation of RR120.

References

[1] B. Hayati, A. Maleki, F. Najafi, H. Daraei, F. Gharibi, G. McKay, Adsorption of Pb^{2+}, Ni^{2+}, Cu^{2+}, Co^{2+} metal ions from aqueous solution by PPI/SiO_2 as new high performance adsorbent: preparation, characterization, isotherm, kinetic, thermodynamic studies, J. Mol. Liq., 237 (2017) 428–436.

[2] B. Hayati, N.M. Mahmoodi, A. Maleki, Dendrimer–titania nanocomposite: synthesis and dye-removal capacity, Res. Chem. Int., 41 (2015) 3743–3757.

[3] N.M. Mahmoodi, B. Hayati, H. Bahrami, M. Arami, Dye adsorption and desorption properties of Mentha pulegium in single and binary systems, J. Appl. Polym. Sci., 122 (2011) 1489–1499.

[4] N.M. Mahmoodi, M. Oveisi, M. Bakhtiari, B. Hayati, A.A. Shekarchi, A. Bagheri, S. Rahimi, Environmentally friendly ultrasound-assisted synthesis of magnetic zeolitic imidazolate framework-Graphene oxide nanocomposites and pollutant removal from water, J. Mol. Liq., 282 (2019) 115–130.

[5] D. En, L. Zheng, X. Yun, B. Bin, M. Yan, J. Juan, F. Li, S. An, Z. Wei, Applied surface science synthesis and photocatalytic property of multilayered Co_3O_4, Appl. Surf. Sci., 355 (2015) 547–552.

[6] A. Ajmal, I. Majeed, N. Malik, Principles and mechanisms of photocatalytic dye degradation on TiO_2 based photocatalysts: a comparative overview, RSC Adv., 4 (2014) 37003–37026.

[7] A. Almasian, M.E. Olya, N.M. Mahmoodi, Synthesis of polyacrylonitrile/polyamidoamine composite nanofibers using electrospinning technique and their dye removal capacity, J. Taiwan Inst. Chem. Eng., 49 (2015) 119–128.

[8] N. Nasrollahi, V. Vatanpour, S. Aber, N.M. Mahmoodi, Preparation and characterization of a novel polyethersulfone (PES) ultrafiltration membrane modified with a CuO/ZnO nanocomposite to improve permeability and antifouling properties, Sep. Purif. Technol., 192 (2018) 369–382.

[9] A. Asghar, A. Aziz, A. Raman, W. Mohd, A. Wan, Advanced oxidation processes for *in-situ* production of hydrogen peroxide/hydroxyl radical for textile wastewater treatment: a review, J. Cleaner Prod., 87 (2015) 826–838.

[10] N.M. Mahmoodi, Nickel ferrite nanoparticle: synthesis, modification by surfactant and dye removal ability, Water Air Soil Pollut., 224 (2013) 1419, doi: 10.1007/s11270–012–1419–7.

[11] N.M. Mahmoodi, J. Abdi, D. Bastani, Direct dyes removal using modified magnetic ferrite nanoparticle, J. Environ. Health Sci. Eng., 12 (2014) 1–10.

[12] N.M. Mahmoodi, Manganese ferrite nanoparticle: synthesis, characterization, and photocatalytic dye degradation ability, Desal. Water Treat., 53 (2015) 84–90.

[13] A.A. Ismail, D.W. Mazyck, Impact of heat treatment and composition of ZnO–TiO_2 nanoparticles for photocatalytic oxidation of an azo dye, Ind. Eng. Chem. Res., 47 (2008) 1483–1487.

[14] N.M. Mahmoodi, J. Abdi, M. Oveisi, M. Alinia Asli, M. Vossoughi, Metal-organic framework (MIL-100 (Fe)): synthesis, detailed photocatalytic dye degradation ability in colored textile wastewater and recycling, Mater. Res. Bull., 100 (2018) 357–366.

[15] N.M. Mahmoodi, Dendrimer functionalized nanoarchitecture: synthesis and binary system dye removal, J. Taiwan Inst. Chem. Eng., 45 (2014) 2008–2020.

[16] A. Naseri, M. Samadi, N.M. Mahmoodi, A. Pourjavadi, H. Mehdipour, A.Z. Moshfegh, Tuning composition of electrospun ZnO/CuO nanofibers: toward controllable and efficient solar photocatalytic degradation of organic pollutants, J. Phys. Chem. C, 121 (2017) 3327–3338.

[17] O. Tavakoli, V. Goodarzi, M.R. Saeb, N.M. Mahmoodi, R. Borja, Competitive removal of heavy metal ions from squid oil under isothermal condition by CR11 chelate ion exchanger, J. Hazard. Mater., 334 (2017) 256–266.

[18] N.M. Mahmoodi, N.Y. Limaee, M. Arami, S. Borhany, M. Mohammad-Taheri, Nanophotocatalysis using nanoparticles of titania. Mineralization and finite element modelling of Solophenyl dye decolorization, J. Photochem. Photobiol., A, 189 (2007) 1–6.

[19] H. You, Z. Wu, Y. Jia, X. Xu, Y. Xia, Z. Han, Y. Wang, High-efficiency and mechano-/photo-bi-catalysis of piezoelectric-ZnO@photoelectric-TiO_2 core-shell nanofibers for dye decomposition, Chemosphere, 183 (2017) 528–535.

[20] A.M. Al-Hamdi, U. Rinner, M. Sillanpää, Tin dioxide as a photocatalyst for water treatment: a review, Process Saf. Environ. Prot., 107 (2017) 190–205.

[21] B. Shi, G. Li, D. Wang, C. Feng, H. Tang, Removal of direct dyes by coagulation: the performance of preformed polymeric aluminum species, J. Hazard. Mater., 143 (2007) 567–574.

[22] X. Wang, J. Jia, Y. Wang, Degradation of C.I. Reactive Red 2 through photocatalysis coupled with water jet cavitation, J. Hazard. Mater., 185 (2011) 315–321.

[23] C. Gao, J. Wang, H. Xu, Y. Xiong, Coordination chemistry in the design of heterogeneous photocatalysts, Chem. Soc. Rev., 46 (2017) 2799–2823.

[24] S. Mozia, Photocatalytic membrane reactors (PMRs) in water and wastewater treatment: a review, Sep. Purif. Technol., 73 (2010) 71–91.

[25] A.O. Juma, E.A.A. Arbab, C.M. Muiva, L.M. Lepodise, G.T. Mola, Synthesis and characterization of CuO-NiO-ZnO mixed metal oxide nanocomposite, J. Alloys Compd., 723 (2017) 866–872.

[26] F. Mustafa, S. Aslam, A. Jamil, M.A. Ahmad, Synthesis and characterization of wide band gap nickel oxide (NiO) powder via a facile route, Optik, 140 (2017) 38–44.

[27] M. Carbone, E. Maria Bauer, L. Micheli, M. Missori, NiO morphology dependent optical and electrochemical properties, Colloids Surf., A, 532 (2017) 178–182.

[28] F. Motahari, M.R. Mozdianfard, F. Soofivand, M. Salavati-Niasari, NiO nanostructures: synthesis, characterization and photocatalyst application in dye wastewater treatment, RSC Adv., 4 (2014) 27654–27660.

[29] D. Zhang, F. Zeng, Visible light-activated cadmium-doped ZnO nanostructured photocatalyst for the treatment of methylene blue dye, J. Mater. Sci., 47 (2012) 2155–2161.

[30] T. Sreethawong, S. Ngamsinlapasathian, S. Yoshikawa, Surfactant-aided sol–gel synthesis of mesoporous-assembled TiO_2-NiO mixed oxide nanocrystals and their photocatalytic azo dye degradation activity, Chem. Eng. J., 192 (2012) 292–300.

[31] A. Hameed, T. Montini, P. Fornasiero, Photocatalytic decolourization of dyes on NiO–ZnO nano-composites, Photochem. Photobiol. Sci., 8 (2009) 677–682.

[32] H. Derikvandi, A. Nezamzadeh-Ejhieh, Synergistic effect of *p-n* heterojunction, supporting and zeolite nanoparticles in enhanced photocatalytic activity of NiO and SnO_2, J. Colloid Interface Sci., 490 (2017) 314–327.

[33] A. Hameed, V. Gombac, T. Montini, M. Graziani, P. Fornasiero, Synthesis, characterization and photocatalytic activity of NiO-Bi_2O_3 nanocomposites, Chem. Phys. Lett., 472 (2009) 212–216.

[34] M. Goudarzi, M. Bazarganipour, M. Salavati-Niasari, Synthesis, characterization and degradation of organic dye over Co_3O_4 nanoparticles prepared from new binuclear complex precursors, RSC Adv., 4 (2014) 46517–46520.

[35] C. Ravi Dhas, R. Venkatesh, K. Jothivenkatachalam, A. Nithya, B. Suji Benjamin, A. Moses Ezhil Raj, K. Jeyadheepan, C. Sanjeeviraja, Visible light driven photocatalytic degradation of Rhodamine B and Direct Red using cobalt oxide nanoparticles, Ceram. Int., 41 (2015) 9301–9313.

[36] M. Roy, S. Ghosh, M.K. Naskar, Ligand-assisted soft-chemical synthesis of self-assembled different shaped mesoporous Co_3O_4: efficient visible light photocatalysts, Phys. Chem. Chem. Phys., 17 (2015) 10160–10169.

[37] S.K. Jesudoss, J. Judith Vijaya, P. Iyyappa Rajan, K. Kaviyarasu, M. Sivachidambaram, L. John Kennedy, H.A. Al-Lohedan, R. Jothiramalingam, M.A. Munusamy, High performance multifunctional green Co_3O_4 spinel nanoparticles: photodegradation of textile dye effluents, catalytic hydrogenation of nitro-aromatics and antibacterial potential, Photochem. Photobiol. Sci., 16 (2017) 766–778.

[38] T.K. Jana, A. Pal, K. Chatterjee, Magnetic and photocatalytic study of Co_3O_4-ZnO nanocomposite, J. Alloys Compd., 653 (2015) 338–344.

[39] X.P. Qiu, J.S. Yu, H.M. Xu, W.X. Chen, W. Hu, G.L. Chen, Interfacial effects of the Cu_2O nano-dots decorated Co_3O_4 nanorods array and its photocatalytic activity for cleaving organic molecules, Appl. Surf. Sci., 382 (2016) 249–259.

[40] X.P. Qiu, J.S. Yu, H.M. Xu, W.X. Chen, W. Hu, H.Y. Bai, G.L. Chen, Interfacial effect of the nanostructured Ag_2S/Co_3O_4 and its catalytic mechanism for the dye photodegradation under visible light, Appl. Surf. Sci., 362 (2016) 498–505.

[41] J. Lv, D. Li, K. Dai, C. Liang, D. Jiang, L. Lu, G. Zhu, Multi-walled carbon nanotube supported CdS-DETA nanocomposite for efficient visible light photocatalysis, Mater. Chem. Phys., 186 (2017) 372–381.

[42] K.E. Tettey, M.Q. Yee, D. Lee, Photocatalytic and conductive MWCNT/TiO_2 nanocomposite thin films, ACS Appl. Mater. Interfaces, 2 (2010) 2646–2652.

[43] G. Sohn, H. Choi, I. Jeon, D.W. Chang, L. Dai, J. Baek, Grafted multiwalled carbon nanotubes as oxygen reduction catalysts, ACS Nano, 6 (2012) 6345–6355.

[44] W. Oh, M. Chen, Synthesis and characterization of CNT/TiO_2 composites thermally derived from MWCNT and titanium(IV) *n*-butoxide, Composites, 29 (2008) 159–164.

[45] V.B. Koli, A.G. Dhodamani, S.D. Delekar, S.H. Pawar, *In situ* sol–gel synthesis of anatase TiO_2-MWCNTs nanocomposites and their photocatalytic applications, J. Photochem. Photobiol., A, 333 (2017) 40–48.

[46] R. Long, Electronic structure of semiconducting and metallic tubes in TiO_2/carbon nanotube heterojunctions: density functional theory calculations, J. Phys. Chem. Lett., 4 (2013) 1340–1346.

[47] S. Sadhu, P. Poddar, Template-free fabrication of highly-oriented single-crystalline 1D-rutile TiO_2-MWCNT composite for enhanced photoelectrochemical activity, J. Phys. Chem. C, 118 (2014) 19363–19373.

[48] R. Zhang, L. Fan, Y. Fang, S. Yang, Electrochemical route to the preparation of highly dispersed composites of ZnO/carbon nanotubes with significantly enhanced electrochemiluminescence from ZnO, J. Mater. Chem., 18 (2008) 4964–4970.

[49] T. Wen, Y. Bin Tang, F.Y. Chen, B.Y. Mo, Preparation, characterization of a ceria loaded carbon nanotubes nanocomposites photocatalyst and degradation of azo dye Acid Orange 7, Arch. Environ. Prot., 42 (2016) 12–19.

[50] H. Kusic, N. Koprivanac, A.L. Bozic, Environmental aspects on the photodegradation of reactive triazine dyes in aqueous media, J. Photochem. Photobiol., A, 252 (2013) 131–144.

[51] Y. Zheng, Y. Yang, Y. Zhang, W. Zou, Y. Luo, L. Dong, B. Gao, Facile one-step synthesis of graphitic carbon nitride-modified biochar for the removal of reactive red 120 through adsorption and photocatalytic degradation, Biochar, 1 (2019) 89–96.

[52] P. Martis, B.R. Venugopal, J. Delhalle, Z. Mekhalif, Selective decoration of nickel and nickel oxide nanocrystals on multiwalled carbon nanotubes, J. Solid State Chem., 184 (2011) 1245–1250.

[53] A.K. Singh, B.P. Panda, S. Mohanty, S.K. Nayak, Study on metal decorated oxidized multiwalled carbon nanotube (MWCNT) - epoxy adhesive for thermal conductivity applications, J. Mater. Sci. - Mater. Electron., 28 (2017) 8908–8920.

[54] W. Wilson, A. Samuel, O.O. Sudheesh, K. Shukla, E. Selorm, A. Poomani, P. Govender, Palladium-doped – ZrO_2 – multiwalled carbon nanotubes nanocomposite: an advanced photocatalyst for water treatment, Appl. Phys. A, 122 (2016) 579, doi: 10.1007/s00339-016-0086-8.

[55] B. Systems, Amino-functionalized carbon nanotubes for binding to polymers and biological systems, Chem. Mater., 17 (2005) 1290–1295.

[56] R. Yudianti, H. Onggo, Y. Saito, T. Iwata, J. Azuma, Analysis of functional group sited on multi-wall carbon nanotube surface, Open Mater. Sci. J., 5 (2011) 242–247.

[57] S.M. Yuen, C.C.M. Ma, Y.Y. Lin, H.C. Kuan, Preparation, morphology and properties of acid and amine modified multiwalled carbon nanotube/polyimide composite, Compos. Sci. Technol., 67 (2007) 2564–2573.

[58] K.A.M. Shanmugharaj, S.H. Ryu, Multiwalled carbon nanotubes-supported Nickel catalysts for the steam reforming of propane, J. Mater. Sci., 47 (2012) 2985–2994.

[59] K. Saravanakumar, M.M. Ramjan, P. Suresh, V. Muthuraj, Fabrication of highly efficient visible light driven Ag/CeO_2 photocatalyst for degradation of organic pollutants, J. Alloys Compd., 664 (2016) 149–160.

[60] S.M. Hosseinpour-Mashkani, A. Sobhani-Nasab, Simple synthesis and characterization of copper tungstate nanoparticles: investigation of surfactant effect and its photocatalyst application, J. Mater. Sci. – Mater. Electron., 27 (2016) 7548–7553.

[61] V. Rajendar, T. Dayakar, B. Satish, K. Subramanyam, Y. Prashanthi, J.N. Technological, synthesis and characterization of Cuins2 nanoparticles as potential candidates for photocatalyst and photovoltaic materials, Chalcogenide Lett., 13 (2016) 467–475.

[62] A. Setyani, S. Wahyuni, S. Priatmoko, E.A.P. Wibowo, N. Amin, Synthesis and characterization of TNTs/polyaniline composite as photocatalyst degradation of Rhodamin B by Visible Light, KnE Life Sci., 3 (2017) 41–50, doi: 10.18502/kls.v3i5.977.

[63] H. Chen, W. Liu, Z. Qin, ZnO/$ZnFe_2O_4$ nanocomposite as a broad-spectrum photo-Fenton-like photocatalyst with near-infrared activity, Catal. Sci. Technol., 7 (2017) 2236–2244.

[64] A. Dolgonos, T.O. Mason, K.R. Poeppelmeier, Direct optical band gap measurement in polycrystalline semiconductors: a critical look at the Tauc method, J. Solid State Chem., 240 (2016) 43–48.

[65] H. Park, S. Liu, P.A. Salvador, G.S. Rohrer, High visible-light photochemical activity of titania decorated on single-wall carbon nanotube, RSC Adv., 6 (2016) 22285–22294.

[66] A. Hameed, V. Gombac, T. Montini, M. Graziani, P. Fornasiero, Synthesis, characterization and photocatalytic activity of NiO–Bi_2O_3 nanocomposites, Chem. Phys. Lett., 472 (2009) 212–216.

[67] E.M. Alrobayi, A.M. Algubili, A.M. Aljeboree, A.F. Alkaim, F.H. Hussein, Investigation of photocatalytic removal and photonic efficiency of maxilon blue dye GRL in the presence of TiO_2 nanoparticles, Part. Sci. Technol., 35 (2017) 14–20.

[68] X.J. Wen, C.G. Niu, M. Ruan, L. Zhang, G.M. Zeng, AgI nanoparticles-decorated CeO_2 microsheets photocatalyst for the degradation of organic dye and tetracycline under visible-light irradiation, J. Colloid Interface Sci., 497 (2017) 368–377.

[69] H. Wang, S. Li, L. Zhang, Z. Chen, J. Hu, R. Zou, K. Xu, G. Song, H. Zhao, J. Yang, J. Liu, Surface decoration of Bi_2WO_6 superstructures with Bi_2O_3 nanoparticles: an efficient method to improve visible-light-driven photocatalytic activity, CrystEngComm, 15 (2013) 9011–9019.

[70] D. Malwal, P. Gopinath, Enhanced photocatalytic activity of hierarchical three dimensional metal oxide@CuO nanostructures towards the degradation of Congo red dye under solar radiation, Catal. Sci. Technol., 6 (2016) 4458–4472.

[71] H.R. Pouretedal, A. Norozi, M.H. Keshavarz, A. Semnani, Nanoparticles of zinc sulfide doped with manganese, nickel and copper as nanophotocatalyst in the degradation of organic dyes, J. Hazard. Mater., 162 (2009) 674–681.

[72] V. Mirkhani, Photocatalytic degradation of Azo dyes catalyzed by Ag doped Tio_2 photocatalyst, J. Iran. Chem. Soc., 6 (2009) 578–587.

[73] C.A.K. Gouvêa, F. Wypych, S.G. Moraes, N. Durán, N. Nagata, P. Peralta-Zamora, Semiconductor-assisted photocatalytic degradation of reactive dyes in aqueous solution, Chemosphere, 40 (2000) 433–440.